

# Preparation of Carbon Nanotubes with Supported Metal Oxide Nanoparticles: Effect of Metal Precursor on Thermal Decomposition Behavior of the Materials

E.V. Matus\*, L.M. Khitsova, O.S. Efimova, S.A. Yashnik, N.V. Shikina, Z.R. Ismagilov

Federal Research Center of Coal and Coal Chemistry SB RAS, 650000, 18 Sovetskiy pr., Kemerovo, Russia

## Article info

*Received:*

17 April 2019

*Received in revised form:*

26 June 2019

*Accepted:*

14 August 2019

## Keywords

Carbon nanomaterial

Nanoparticles

Catalyst

Thermal analysis

## Abstract

To develop new catalysts based on carbon nanomaterials with supported metal oxide nanoparticles for oxidative transformations of sulfur compounds, a series of metal oxide nanoparticle-decorated carbon nanotubes ( $\text{MO}_x/\text{CNTs}$ ) were prepared by incipient wetness impregnation at a variation of the active metal type ( $M = \text{Ce}, \text{Mo}, \text{Cu}$ ). The thermal decomposition of bulk and CNT supported metal precursors used in the preparation of  $\text{MO}_x/\text{CNTs}$  was analyzed under inert atmosphere employing several thermoanalytical techniques (thermogravimetry, differential thermogravimetry and differential scanning calorimetry) coupled with mass spectrometry. The thermolysis parameters of the bulk and supported metal precursors were compared and the effect of CNT support on the decomposition pattern of compounds was elucidated. It was established that the decomposition of metal precursors supported on CNTs was started and completed at temperatures of 15–25 and 25–70 °C lower, respectively, compared with the bulk active metal precursor. The enhancement of CNT support stability against thermal degradation is observed in the following row of metal cations:  $\text{Ce} < \text{Cu} < \text{Mo}$  < pristine and metal anions of precursor: nitrate < chloride < sulfate. The optimal mode of thermal treatment of catalyst and appropriate active metal precursors were selected for advanced synthesis of nanosized  $\text{MO}_x/\text{CNT}$  catalyst.

## 1. Introduction

The supported metal nanoparticles and nano-clusters are effective catalytic systems in various catalysis processes [1–3]. A decrease in particle size to a nanometer level leads to a change in their melting temperature, heat capacity, thermal conductivity, and the appearance of unique electronic, optical, and magnetic properties. Due to specific physicochemical properties and a high concentration of coordination-unsaturated centers, nanocatalysts have unique functional properties, combining high activity and selectivity. The metal-support interaction is one of the key factors determining the properties of supported metal-containing particles [4, 5]. In particular, the chemical composition of the support can affect the size, morphology, electronic and redox properties of supported metal-contain-

ing particles and, accordingly, their catalytic properties [6, 7]. Carbon nanomaterials (CNMs), e.g. active carbon, carbon nanotubes (CNTs), carbon nanofibres (CNFs), graphite carbon (GC), of different structure are successfully used as supports for catalytically active metal and oxide particles and utilized in various catalytic processes such as preferential oxidation of carbon monoxide, methanol electrooxidation, dry reforming of methane, ammonia decomposition [2, 8–16]. In contrast to oxide supports, they have hydrophobic surface that provides good miscibility in model oil and promote the sulfidation process due to the limited metal-support interaction [9]. These properties of CNMs, as well as adsorption capacity, the absence of strong acid sites and ability to activate oxygen have drawn attention to their use in the process of selective oxidation of sulfur-containing compounds in fuels [17–23]. In contrast to oxide supports for which different compositions of active components

\*Corresponding author. E-mail: [matus@catalysis.ru](mailto:matus@catalysis.ru)

were studied and favorable compositions were selected [24–27] the open literature on supported active species on CNMs for oxidative desulfurization is quite limited and their optimal type, content and dispersion is not fully understood so far.

Various techniques were developed to modify the CNMs by metal or oxide nanoparticles: traditional wet chemistry routes (impregnation, adsorption, precipitation) [14, 28–31], thermal decomposition [32], electrochemical deposition [33], hydrothermal synthesis [18], as well as more specific procedures using laser ablation in liquid [34, 35] or microwave irradiation [15]. Among the wide range of functionalization strategies one the simplest consists of impregnation of carbon material with a solution of a metal oxide precursor with the subsequent thermal treatment. It is obvious that the precursor type and mode of thermolysis of metal-modified CNMs affect the physicochemical and functional properties of the nanocomposite. It was shown that the decomposition of supported compounds depends on the support nature and can be delayed or enhanced compared with the bulk compounds [36, 37]. On the other hand, the stability of CNMs to degradation can be changed in the presence of metal-containing compounds [38, 39]. So the selection of the appropriate metal precursor and mode of thermal treatment of nanocomposite is required for the successful synthesis of CNMs with supported metal oxide nanoparticles.

In this paper with the aim to develop new catalysts based on CNMs with supported metal oxide nanoparticles for oxidative transformations of sulfur compounds, a series of metal oxide nanoparticle-decorated carbon nanotubes ( $\text{MO}_x/\text{CNTs}$ ,  $M = \text{Ce}, \text{Mo}, \text{Cu}$ ) were prepared by incipient wetness impregnation and studied by thermoanalytical techniques (TA) coupled with mass spectrometry. The effect of the CNT support on the decomposition pattern of metal precursors, used in the preparation of  $\text{MO}_x/\text{CNTs}$ , as well as the influence of modification on the thermal properties of CNTs was elucidated.

## 2. Experimental

### 2.1. Catalyst preparation

The CNTs «Taunit» were used in this work as supports. They were purchased from NanoTech-Center Ltd. (Tambov, Russia) and utilized as received without any further purification. The CNTs were multi-walled nanotubes with an inner diameter 10–20 nm and a specific surface area 180  $\text{m}^2/\text{g}$ .

Their physicochemical properties were given and discussed in [40].

The  $\text{MO}_x/\text{CNT}$  catalysts were prepared by incipient wetness impregnation of a CNT support with solutions of active metal precursors. Unless otherwise specified, aqueous solutions of metal salts have been applied. The following salts of analytical grade were used as active metal precursor: cerium nitrate hexahydrate  $\text{Ce}(\text{NO}_3)_3 \cdot 6\text{H}_2\text{O}$ , cerium chloride heptahydrate  $\text{CeCl}_3 \cdot 7\text{H}_2\text{O}$ , ammonium cerium (IV) nitrate  $(\text{NH}_4)_2\text{Ce}(\text{NO}_3)_6$  as cerium precursors; copper nitrate trihydrate  $\text{Cu}(\text{NO}_3)_2 \cdot 3\text{H}_2\text{O}$ , copper sulfate pentahydrate  $\text{CuSO}_4 \cdot 5\text{H}_2\text{O}$ , copper chloride dihydrate  $\text{CuCl}_2 \cdot 2\text{H}_2\text{O}$  as copper precursors; ammonium paramolybdate tetrahydrate  $(\text{NH}_4)_6\text{Mo}_7\text{O}_{24} \cdot 4\text{H}_2\text{O}$  as a molybdenum precursor. In addition, citrate complexes of metals were used as metal precursors. For this, the appropriate metal salt ( $\text{Ce}(\text{NO}_3)_3 \cdot 6\text{H}_2\text{O}$ ,  $\text{Cu}(\text{NO}_3)_2 \cdot 3\text{H}_2\text{O}$  or  $(\text{NH}_4)_6\text{Mo}_7\text{O}_{24} \cdot 4\text{H}_2\text{O}$ ) was mixed with the required content of a solution of citric acid in ethylene glycol. The obtained viscous solution was used for the impregnation of a CNT support. After impregnation, the samples were dried for 6 h at 80 °C. The metal content was constant and equal to 10 wt.%.

### 2.2. Characterization of catalysts

The thermogravimetry (TG), differential thermogravimetry (DTG) and differential scanning calorimetry (DSC) analyses were carried out in an STA 449 F3 Jupiter® thermal analyzer (NETZSCH Gerätebau GmbH, Germany). The samples of mass about 8 mg were heated in the platinum crucible from 25 up to 1000 °C in  $\text{N}_2$  atmosphere at a heating rate 5°/min.

This apparatus for the thermal analysis was connected on-line with a mass spectrometer (MS) QMS 403 C Aëolos so that parallel analysis of gaseous products of the decomposition was carried out. The energy of the ion source was 80 eV and the CH-TRON detector was used. Ion currents for  $M/q$  values ( $M$  – molecular mass of a particle,  $q$  – particle charge) were monitored. Selected  $M/q$  values correspond to the molecular and fragmentation ions which can be formed during the decomposition of the metal precursor and CNT support. All intensities of ion peaks were first corrected for the background.

## 3. Results and Discussions

TG, DTA, DSC and MS curves of CNTs «Taunit» are depicted in Fig. 1.

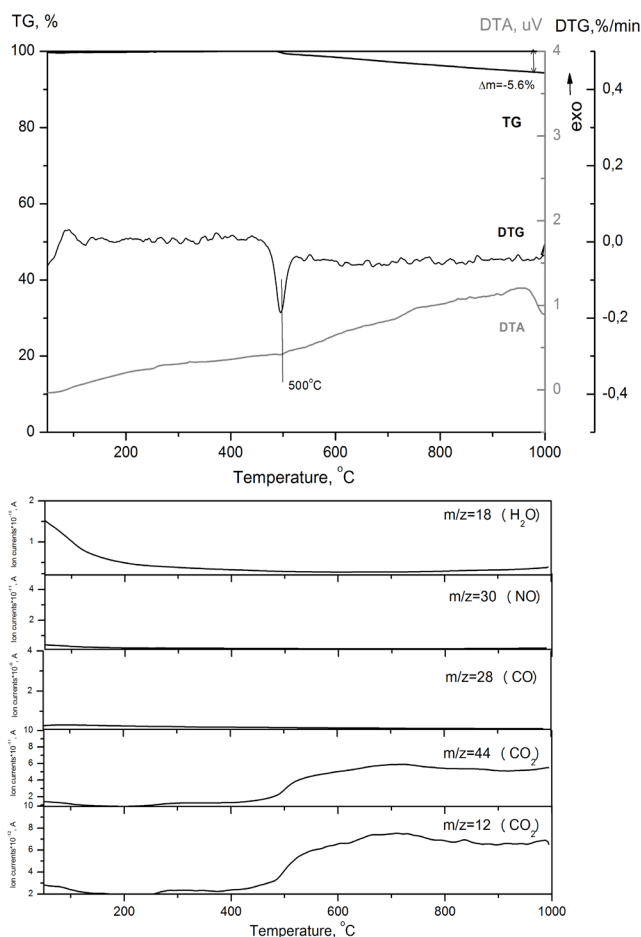


Fig. 1. TG, DTG, DSC and MS curves of CNTs «Taunit».

CNTs are thermally stable up to 500 °C: there are no phase change or decomposition reactions. Between 500 and 1000 °C the 5.6% weight loss

occurs due to the sublimation of surface O-containing functional groups, the main gaseous product is CO<sub>2</sub> as it was shown by MS-analysis. The weight loss is not accompanied by any thermal effects (Fig. 1). It is an important result showing the possibility of their use as supports for metal oxides at preparation of nanoparticle-decorated carbon nanotubes MO<sub>x</sub>/CNTs.

Three types of metals as an active component in MO<sub>x</sub>/CNT materials were considered in this study: Ce, Cu and Mo. The abbreviation of samples and precursor type used for the synthesis of MO<sub>x</sub>/CNT materials are listed in Table 1. During thermal treatment of as-prepared samples under inert atmosphere from room temperature to 1000 °C, the thermal decomposition of the metal precursor supported on CNTs as well as the degradation of the carbon matrix are expected. We calculated the expected mass loss during thermal analysis due to the precursor decomposition, suggesting the formation of the corresponding metal oxides (Table 1).

The expected weight loss of the sample during the decomposition of non-supported (bulk) metal precursors to oxides varies from 20 to 90 wt.%. This value is determined by the ratio of molecular weights of the corresponding compounds. For the supported precursors, such an expected weight loss is less and is in the range of 3–65 wt.%. In both cases, among the samples studied, weight loss is minimal when using ammonium paramolybdate as a metal precursor, and maximum when using metal citrate complexes.

**Table 1**

The abbreviation of samples, precursor type used for the synthesis of MO<sub>x</sub>/CNT materials, and expected mass loss during thermal analysis due to precursor decomposition

Sample abbreviation	Precursor type	Expected composition of product of thermal decomposition of bulk and supported precursor	Expected mass loss during thermal analysis due to precursor decomposition, wt.%	
			Bulk precursor	Supported precursor
Ce/CNT-N	Ce(NO <sub>3</sub> ) <sub>3</sub> ·6H <sub>2</sub> O	CeO <sub>2</sub>	60.4	15.5
Ce/CNT-C	CeCl <sub>3</sub> ·7H <sub>2</sub> O	CeO <sub>2</sub>	53.8	12.5
Ce/CNT-A	(NH <sub>4</sub> ) <sub>2</sub> Ce(NO <sub>3</sub> ) <sub>6</sub>	CeO <sub>2</sub>	68.6	21.2
Ce/CNT-Cit	Citrate complex	CeO <sub>2</sub>	93.8	65.0
Cu/CNT-N	Cu(NO <sub>3</sub> ) <sub>2</sub> ·3H <sub>2</sub> O	CuO	67.1	20.3
Cu/CNT-C	CuCl <sub>2</sub> ·2H <sub>2</sub> O	CuO	53.3	12.5
Cu/CNT-S	CuSO <sub>4</sub> ·5H <sub>2</sub> O	CuO	68.1	21.1
Cu/CNT-Cit	Citrate complex	CuO	93.9	65.8
Mo/CNT-P	(NH <sub>4</sub> ) <sub>6</sub> Mo <sub>7</sub> O <sub>24</sub> ·4H <sub>2</sub> O	MoO <sub>3</sub>	18.5	3.3

### 3.1. Ce/CNTs

Figure 2 demonstrates the behaviors of decomposition of  $\text{Ce}(\text{NO}_3)_3 \cdot 6\text{H}_2\text{O}$  (a) and Ce/CNT-N (b) in inert atmosphere. According to the obtained data (Fig. 1a), the decomposition of bulk  $\text{Ce}(\text{NO}_3)_3 \cdot 6\text{H}_2\text{O}$  proceeds through several steps including the two-stage dehydration process, the formation of anhydrous cerium nitrate and its transformation during which the oxidation of Ce(III) by the nitrate ion with the formation of  $\text{CeO}_2$  occurs [41]. The three weight losses are observed at  $T_{\text{DTG}} = 95, 195$  and  $240$  °C, accompanied by pronounced endothermic effects. The evolved gas during the first and second stages is identified as water ( $m/z = 18$ ) while the third stage is characterized by evolution of nitrogen oxides ( $m/z = 30, 46$ ). The total mass loss ( $\Delta m_{\Sigma} = 58.4 \pm 0.5\%$ ) agrees satisfactorily with the theoretical mass loss (60.4%, Table 1) to form  $\text{CeO}_2$ .

The decomposition of supported  $\text{Ce}(\text{NO}_3)_3 \cdot 6\text{H}_2\text{O}$  also proceeds over three stages but has some distinctive features (Fig. 2b). The decomposition of

the salt begins at lower temperatures ( $T_{\text{DTG1}} = 80$  vs.  $95$  °C), other  $T_{\text{DTG}}$  have a similar shift. This trend also applies to the evolution of nitrogen oxides. The mass loss in the temperature range between 25 and  $400$  °C ( $15.0 \pm 0.5\%$ ) agrees approximately with the expected value (Table 1). In addition, the weight loss (25%) without exothermic phenomena is observed at a temperature range between  $400$  and  $1000$  °C. It is accompanied by the release of  $\text{CO}_2$  in the gas phase (Fig. 2b). This indicates a significant degradation of the carbon matrix of CNTs in the presence of oxidizing agents – nitrogen oxides, formed during the decomposition of supported  $\text{Ce}(\text{NO}_3)_3 \cdot 6\text{H}_2\text{O}$ .

Table 2 summarizes the data of TA and MS analysis for all precursors and Ce/CNT samples. Taking into account the literature data and research results [42–49], we can conclude that in comparison with bulk salts for supported salts the temperature region of the salt decomposition shifts to the low-temperature region. The decomposition of metal precursors supported on CNTs was started and completed at temperatures of lower by 15–10

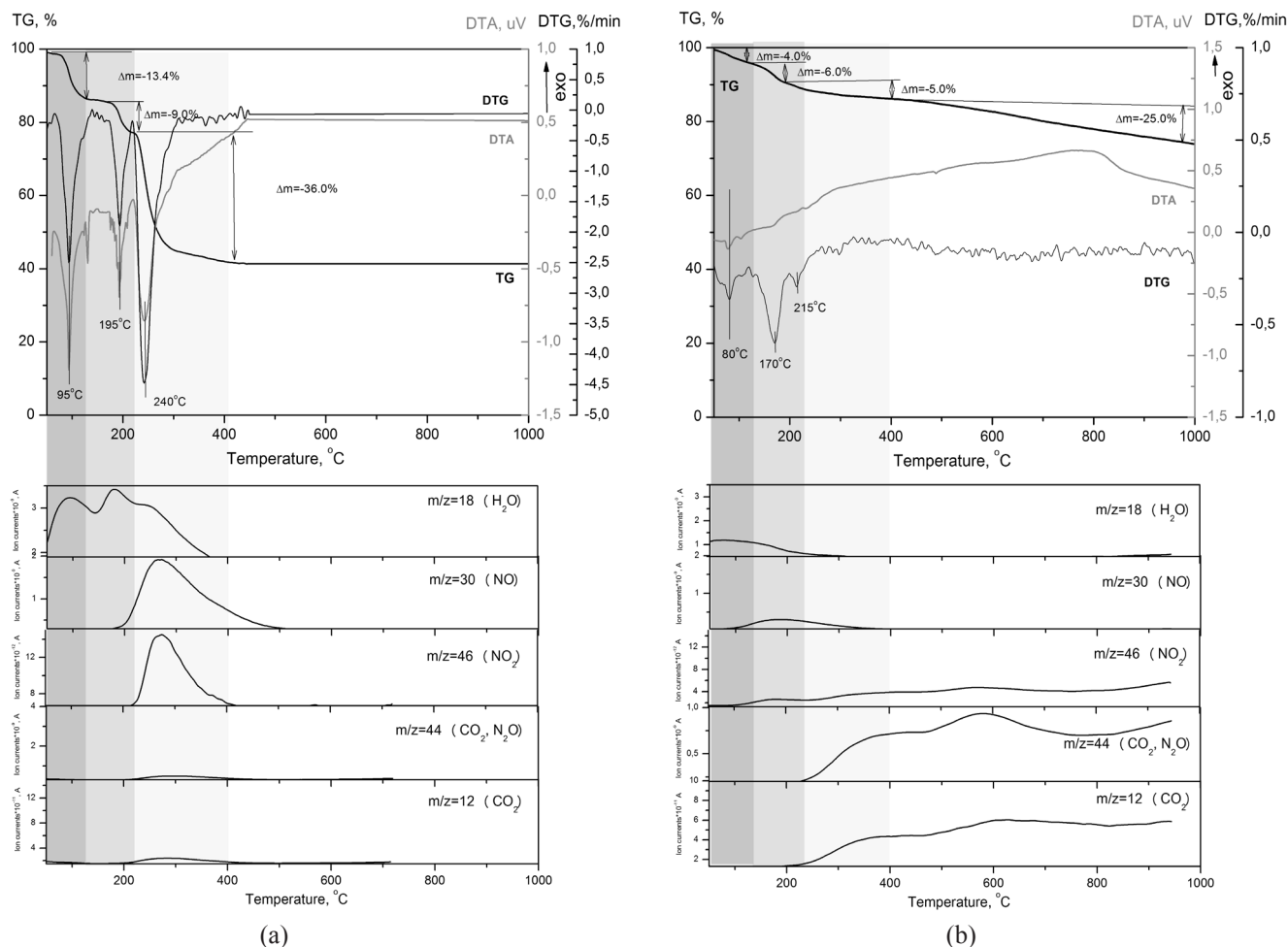


Fig. 2. TG, DTG, DSC and MS curves of bulk (a) and CNT supported (b)  $\text{Ce}(\text{NO}_3)_3 \cdot 6\text{H}_2\text{O}$ .

**Table 2**  
TA and MS data for the decomposition of bulk and CNT supported Ce precursor

Sample	Weight loss ( $\Delta m_i$ ), corresponding to the different stage of decomposition (range of $\Delta T$ , °C), and total weight loss ( $\Delta m_{\Sigma}$ ) at 1000 °C, %					DTG peak temperature and type of thermal effect (exo/endo), °C					Evolved gas products in different temperature ranges ( $\Delta T$ , °C)	
	$\Delta m_1$	$\Delta m_2$	$\Delta m_3$	$\Delta m_4$	$\Delta m_5$	$\Delta m_{\Sigma}$	T <sub>1</sub>	T <sub>2</sub>	T <sub>3</sub>	T <sub>4</sub>		T <sub>5</sub>
Ce(NO <sub>3</sub> ) <sub>3</sub> ·6H <sub>2</sub> O	13.4 (25-130)	9.0 (130-230)	36.0 (230-400)	-	-	58.4	95 endo	195 endo	240 endo	-	-	H <sub>2</sub> O (25-400) NO <sub>x</sub> (200-400)
Ce/CNT-N	4.0 (25-130)	6.0 (130-230)	5.0 (230-400)	25.0 (400-1000)	-	40.0	80 endo	170 endo	215	-	-	H <sub>2</sub> O (25-400) NO <sub>x</sub> (100-400) CO <sub>2</sub> (230-1000)
CeCl <sub>3</sub> ·7H <sub>2</sub> O	15.6 (25-95)	5.9 (95-115)	7.1 (115-155)	5.9 (155-400)	17.9 400-900	52.4	85 endo	110 endo	125 endo	165 endo	-	H <sub>2</sub> O (25-300) HCl (25-200, 500-1000)
Ce/CNT-C	5.8 (25-105)	4.0 (105-500)	8.9 (500-1000)	-	-	18.7	60 endo	135 endo	575	-	-	H <sub>2</sub> O (25-200) HCl, Cl <sub>2</sub> (200-1000) CO <sub>2</sub> (300-1000)
(NH <sub>4</sub> ) <sub>2</sub> Ce(-NO <sub>3</sub> ) <sub>6</sub>	28.3 (25-245)	38.8 (245-400)	-	-	-	67.1	220 endo	235 endo	270 endo	-	-	H <sub>2</sub> O, NH <sub>3</sub> (25-400) NO <sub>x</sub> (200-400)
Ce/CNT-A	3.9 (25-110)	3.0 (110-165)	15.0 (165-330)	7.2 (330-1000)	-	28.9	60 endo	140 endo	200 exo	-	-	H <sub>2</sub> O, NH <sub>3</sub> (25-350) NO <sub>x</sub> (150-350) CO <sub>2</sub> (150-1000)
Citrate complex	5.3 (25-100)	18.3 (100-125)	26.7 (125-225)	16.0 (225-280)	19.5 (280-670)	85.8	105 exo	165 endo	270 endo	-	-	H <sub>2</sub> O (25-700) NO <sub>x</sub> (50-700) CO <sub>2</sub> (50-700)
Ce/CNT-Cit	3.3 (25-120)	16.8 (120-250)	22.4 (250-420)	14.8 (420-700)	-	72.3	60	210	280 exo	365 exo	-	H <sub>2</sub> O (25-550) NO <sub>x</sub> (150-550) CO <sub>2</sub> (150-1000)

and 25–50 °C, respectively, compared with the bulk active metal precursor. This can be connected with higher dispersion of supported salt particles, low concentration of functional groups on the support surface and, consequently a weak metal-support interaction [36]. Comparing the values of the expected (Table 1) and experimentally obtained (Table 2) weight loss of the sample allows us to estimate the degree of the CNT matrix degradation during the thermal treatment of the nanocomposite. Figure 3 shows the temperature of the beginning of CO<sub>2</sub> evolution as well as the weight loss due to the oxidation/decomposition of CNT support during the thermal treatment of the nanocomposite.

Obviously, the presence of salt-containing agents capable of redox reactions provokes a significant shift of degradation of the carbon matrix to the low-temperature region. In particular, using as metal precursors CeCl<sub>3</sub>·7H<sub>2</sub>O, Ce(NO<sub>3</sub>)<sub>3</sub>·6H<sub>2</sub>O or (NH<sub>4</sub>)<sub>2</sub>Ce(NO<sub>3</sub>)<sub>6</sub> salts reduces the temperature of CO<sub>2</sub> evolution start from 500 (found for pristine CNTs) to 300, 230 and 150 °C respectively. According to the weight loss, the degree of CNT support degradation decreases in the following row

of samples: Ce/CNT-N < Ce/CNT-A < Ce/CNT-C < pristine.

Thus the application of CeCl<sub>3</sub>·7H<sub>2</sub>O preserves the CNT matrix from degradation best but makes impossible to form supported cerium oxide during the thermal treatment up to 600 °C due to the stability of CeCl<sub>3</sub> in an inert atmosphere. When using (NH<sub>4</sub>)<sub>2</sub>Ce(NO<sub>3</sub>)<sub>6</sub> salt, the lowest temperature of the beginning of the degradation of the CNT support is observed at the medium values of the weight loss. The Ce(NO<sub>3</sub>)<sub>3</sub>·6H<sub>2</sub>O precursor is characterized by a medium temperature at which the CNT degradation starts, while it has the maximum weight loss due to the oxidation/decomposition of the CNT support during the thermal treatment of the nanocomposite. However, using a low temperature for the Ce/CNT thermal treatment (< 500 °C) provides both the decomposition of supported Ce(NO<sub>3</sub>)<sub>3</sub>·6H<sub>2</sub>O salts to CeO<sub>2</sub> and the protection of the CNT support from the destruction. In addition, these salts are characterized by high solubility, which is necessary for the preparation of catalysts with a high content of active components.

### 3.2. Cu/CNTs

The behaviors of decomposition of Cu(NO<sub>3</sub>)<sub>3</sub>·3H<sub>2</sub>O (a) and Cu/CNT-N (b) in the inert atmosphere are shown in Fig. 4. Bulk Cu(NO<sub>3</sub>)<sub>3</sub>·3H<sub>2</sub>O decomposes by several stages. As can be seen in Fig. 4a, there are four steps with T<sub>DTG</sub> = 120, 200, 265 and 875 °C which are accompanied by pronounced endothermal effects. The main mass loss of the sample occurs up to 300 °C. According to MS data, at the first stage, the water is the main gas product, while nitrogen oxides start to evolve at 120 °C. At the next stage, the dehydration proceeds with the concomitant decomposition of the nitrate group. The third stage is characterized by predominant evolution of NO<sub>x</sub> (m/z = 30, m/z = 46). Further thermal decomposition of the compound is not accompanied by significant emissions of gaseous products. However, the change in sample weight in the high-temperature region indicates its further transformations. The total weight loss is 70.9%, which is somewhat higher than the expected value (Table 1). According to the literature [36, 49, 50], the decomposition of Cu(NO<sub>3</sub>)<sub>3</sub>·3H<sub>2</sub>O leads to the formation of Cu<sub>2</sub>(OH)<sub>3</sub>NO<sub>3</sub> or 3Cu(NO<sub>3</sub>)<sub>2</sub>·Cu(OH)<sub>2</sub> as intermediate products, and the final product CuO can be obtained at 180–310 °C. Apparently, further heating of CuO in an inert atmosphere leads to the

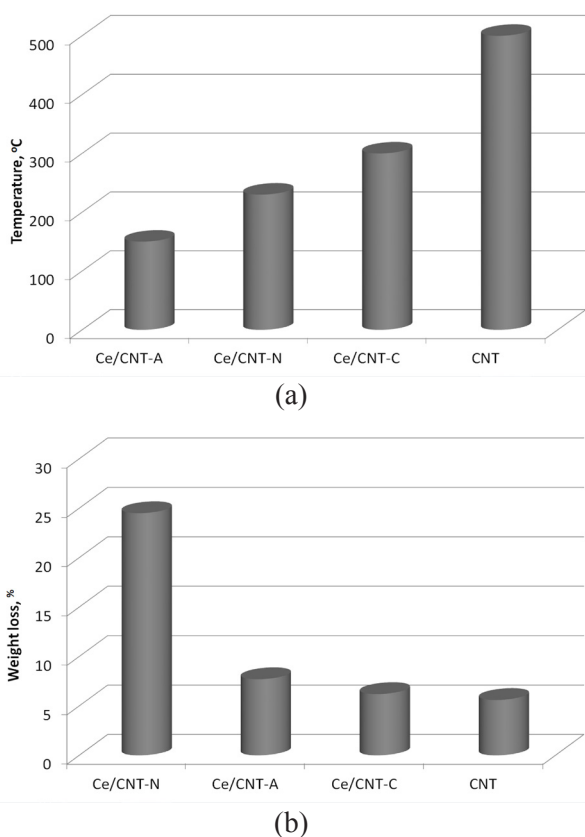


Fig. 3. Temperature of the beginning of CO<sub>2</sub> evolution (a) and weight loss (b) due to the oxidation/decomposition of CNT support during the thermal treatment of the nanocomposite: effect of Ce precursor type.

formation of  $\text{Cu}_2\text{O}$ . Indeed, in this case, the estimated weight loss is 70.4%, which correlates well with the experimentally obtained value.

The thermal decomposition of supported  $\text{Cu}(\text{NO}_3)_2 \cdot 3\text{H}_2\text{O}$  demonstrates a multistage process with overlapping steps with  $T_{\text{DTG}} = 245$  and  $570$  °C (Fig. 4b). The dehydration starts at room temperature and finishes at about  $400$  °C. Before completing dehydration, the decomposition of the nitrate group begins. Between  $200$  and  $400$  °C the evolution of  $\text{H}_2\text{O}$  ( $m/z = 18$ ) with  $\text{NO}_x$  ( $m/z = 30$ ,  $m/z = 46$ ) is observed in MS spectra. The maximum emission of these gases occurs at  $250$  °C, which is similar to those of bulk material. Nevertheless, the weight loss of the sample at  $400$  °C is only  $\Delta m = 12\%$ , which is lower than the expected value (Table 1). The continued emission of nitrogen oxides in the high-temperature region confirms the broadening of the temperature ranges of the decomposition process for CNT supported  $\text{Cu}(\text{NO}_3)_2 \cdot 3\text{H}_2\text{O}$  (Fig. 4). It is important to note that the second endothermic peak related to the  $\text{Cu}_2\text{O}$

formation process for a bulk sample is, on the contrary, shifted to the low-temperature region ( $875 \rightarrow 570$  °C). This expected effect of the CNT support is associated with its reducing potential. The transformation of  $\text{CuO}$  into  $\text{Cu}_2\text{O}$  and further into  $\text{Cu}$  has been previously described for copper nitrate deposited on activated carbon fibers [14]. The difference between the expected mass loss (20.3%, Table 1) and the observed one ( $\Delta m_{\Sigma} = 25.4\%$ ) is about 5% and may be associated with the degradation of the carbon matrix. According to MS data,  $\text{CO}_2$  begins to evolve into the gas phase at a temperature as low as  $200$  °C. Apparently, the presence of highly reactive nitrogen oxides that enter into redox reactions with the carbon of the support contributes to this.

Table 3 contains information for a series of copper-containing samples. The analysis of these results, taking into account literature data [52–56], showed that the effect of the support on the decomposition profile of salts corresponds to the shift of the decomposition temperature region and, especially following  $\text{Cu}^{2+}$  reduction, into the

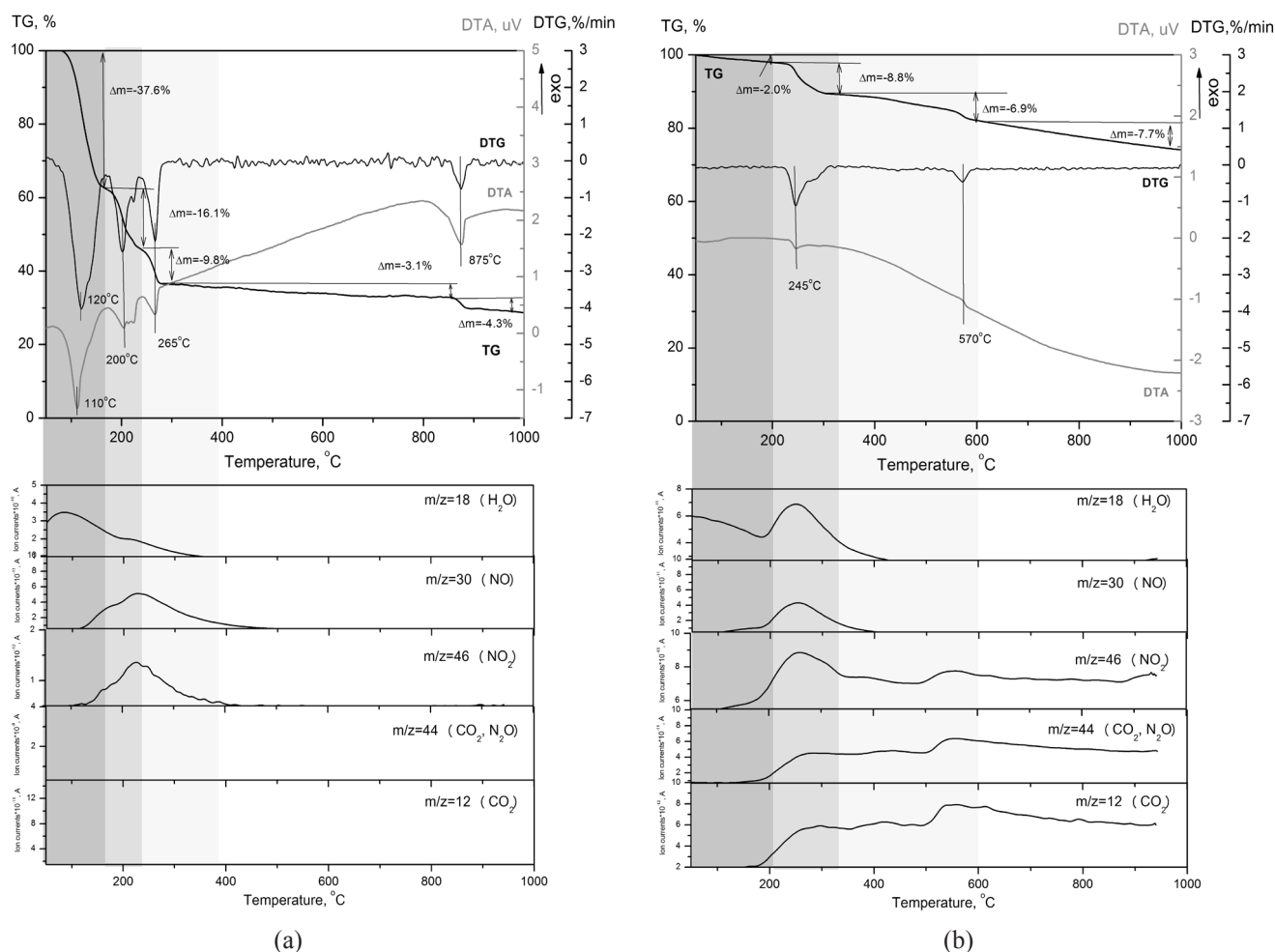


Fig. 4. TG, DTG, DSC and MS curves of bulk (a) and CNT supported (b)  $\text{Cu}(\text{NO}_3)_2 \cdot 3\text{H}_2\text{O}$ .

low-temperature region. The comparison of the beginning of CO<sub>2</sub> evolution and weight loss due to the oxidation/decomposition of the CNT support during the thermal treatment of the nanocomposite is shown in Fig. 5. For the Cu-containing system, the temperature at which the support degradation begins estimated from the beginning of CO<sub>2</sub> evolution increases in the following sequence of samples: Cu/CNT-N = Cu/CNT-C < Cu/CNT-S < pristine. Apparently, the reduced stability of the sample can be associated with the formation of Cu<sub>2</sub>OCl<sub>2</sub> at intermediate stages and the release of O<sub>2</sub>. In the case of the Cu/CNT-N sample, the oxidizing agents are nitrogen oxides released during the salt decomposition. A feature of the Cu/CNT-N and Ce/CNT-S system is easy reducibility of Cu<sup>2+</sup> to Cu<sup>+</sup> and Cu<sup>0</sup> under heat treatment in an inert atmosphere that contributes to a decrease in the rate of the degradation of the CNT (Fig. 5b). The low decomposition temperature of copper nitrate and the stability of the carbon matrix in its presence allow us to recommend the use of this precursor for the synthesis of Cu/CNTs materials.

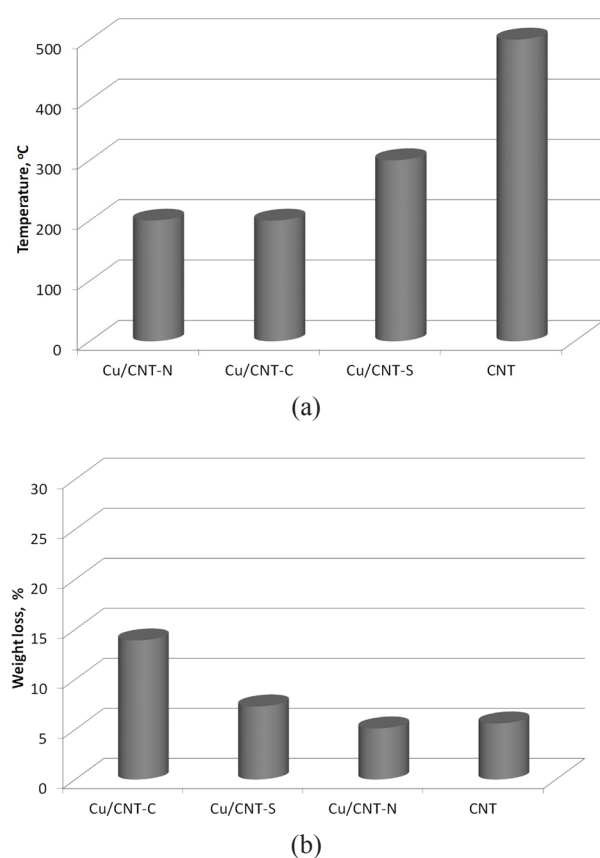


Fig. 5. Temperature of the beginning of CO<sub>2</sub> evolution (a) and weight loss (b) due to the oxidation/decomposition of CNT support during the thermal treatment of the nanocomposite: effect of Cu precursor type.

### 3.3. Mo/CNTs

Figure 6 shows the mode of the decomposition of (NH<sub>4</sub>)<sub>6</sub>Mo<sub>7</sub>O<sub>24</sub>·4H<sub>2</sub>O (a) and Mo/CNT-P (b) in an inert atmosphere. For the bulk (NH<sub>4</sub>)<sub>6</sub>Mo<sub>7</sub>O<sub>24</sub>·4H<sub>2</sub>O compound the process includes five stages with T<sub>DTA</sub> = 95, 120, 200, 295 and 380 °C. All stages, except the second, are accompanied by endothermic effects (Fig. 6). In the stages I and II (T < 160 °C), H<sub>2</sub>O (m/z = 18) and NH<sub>3</sub> (m/z = 18) are evolved in gas phase. The third stage (160 < T < 250 °C) is different by a small amount of volatile products and a slight weight loss (Δm = 2%). H<sub>2</sub>O, NH<sub>3</sub> and NO<sub>x</sub> (m/z = 30, 44, 46) are observed in the gas products at the final decomposition steps (250 < T < 500 °C). It is assumed [57] that NO<sub>x</sub> is formed as a result of the oxidation of evolved NH<sub>3</sub> by the oxygen contained at the trace level in the inert. The total weight loss in the temperature region up to 500 °C is equal to 18.1 and agrees well with the calculated value of 18.5 (Table 1). It indicates the formation MoO<sub>3</sub> in a medium temperature range. The presented results are in good accordance with the proposed decomposition scheme of (NH<sub>4</sub>)<sub>6</sub>Mo<sub>7</sub>O<sub>24</sub>·4H<sub>2</sub>O in an inert atmosphere [57, 58]. It is noted that the heating of the sample to a temperature above 700 °C leads to significant mass loss, indicated by TG results (Fig. 6). This effect is related to the process of sublimation of MoO<sub>3</sub> [59, 60]. The MoO<sub>3</sub> is characterized by rather low temperatures of sublimation and can form complex polymers (MoO<sub>3</sub>)<sub>n</sub>, n = 3–5 in the gaseous phase [60].

The decomposition of CNT supported (NH<sub>4</sub>)<sub>6</sub>Mo<sub>7</sub>O<sub>24</sub>·4H<sub>2</sub>O has four stages (Fig. 6b). At the first two stages at T < 450 °C, a slight weight loss (Δm = 3.5%) without any thermal effects is observed. In this region up to T = 230 °C, H<sub>2</sub>O (m/z = 18) and NH<sub>3</sub> (m/z = 18) are detected in the gas products, then at a temperature of 230–450 °C, the evolution of NO (m/z = 30) additionally occurs. The expected weight loss due to the salt decomposition is equal to 3.3% (Table 1). So the value of the weight loss and the composition of the gas phase indicate that supported (NH<sub>4</sub>)<sub>6</sub>Mo<sub>7</sub>O<sub>24</sub>·4H<sub>2</sub>O has been transformed to oxide at 450 °C. A large weight loss (Δm = 29.6%) is apparent at a higher temperature (Fig. 6b). It is accompanied by CO<sub>2</sub> (m/z = 44, m/z = 12) emission and can relate to the degradation of the CNT support. The sublimation of molybdenum oxide can also contribute to the weight loss of the sample at temperatures above 800 °C. The source of NO<sub>2</sub> (m/z = 46) in the gas phase at T = 300–1000 °C is not clear, and additional studies are required to explain this result.

**Table 3**  
TA and MS data for the decomposition of bulk and CNT supported Cu precursor

Sample	Weight loss ( $\Delta m_i$ ), corresponding to the different stage of decomposition (range of $\Delta T$ , °C), and total weight loss ( $\Delta m_{\Sigma}$ ) at 1000 °C, %					DTG peak temperature and type of thermal effect (exo/endo), °C					Evolved gas products in different temperature ranges ( $\Delta T$ , °C)	
	$\Delta m_1$	$\Delta m_2$	$\Delta m_3$	$\Delta m_4$	$\Delta m_5$	$\Delta m_{\Sigma}$	$T_1$	$T_2$	$T_3$	$T_4$		$T_5$
$\text{Cu}(\text{NO}_3)_2 \cdot 3\text{H}_2\text{O}$	37.6 (25-165)	16.1 (165-245)	9.8 (245-300)	3.1 (300-860)	4.3 (860-1000)	70.9	120 endo	200 endo	265 endo	875 endo		$\text{H}_2\text{O}$ (25-300) $\text{NO}_x$ (120-400)
Cu/CNT-N	2.0 (25-200)	8.8 (200-320)	6.9 (220-600)	7.7 (625-1000)		25.4	245 endo	570 endo				$\text{H}_2\text{O}$ (25-400) $\text{NO}_x$ (200-1000) $\text{CO}_2$ (200-1000)
$\text{CuCl}_2 \cdot 2\text{H}_2\text{O}$	19.8 (25-130)	21.1 (130-485)	54.2 (485-665)	0.9 (665-1000)		96.0	95 endo	455 endo	580 endo			$\text{H}_2\text{O}$ (25-240) $\text{HCl}$ (25-500)
Cu/CNT-C	3.6 (25-95)	1.4 (95-205)	1.3 (205-280)	20.1 (280-1000)		26.4	65 endo	180 endo	230 endo			$\text{H}_2\text{O}$ (25-300) $\text{HCl}$ (25-300) $\text{CO}_2$ (200-1000)
$\text{CuSO}_4 \cdot 5\text{H}_2\text{O}$	12.1 (25-85)	14.7 (85-125)	8.1 (125-275)	32.1 (275-750)	4.1 (750-1000)	71.1	75, 105 endo	220 endo	680 endo	725 endo	855 endo	$\text{H}_2\text{O}$ (25-300) $\text{SO}_2$ (600-1000)
Cu/CNT-S	4.0 (25-80)	3.3 (80-125)	1.9 (125-300)	12.3 (300-600)	6.9 (600-1000)	28.4	70 endo	85 endo	240 endo	475 endo	650 endo	$\text{H}_2\text{O}$ (25-400) $\text{SO}_2$ (400-1000) $\text{CO}_2$ (300-1000)
Citrate complex	35.3 (25-160)	4.7 (160-200)	9.7 (200-250)	20.3 (250-400)	15.8 (400-1000)	95.8	130 endo	190 endo	210 endo	305 endo	-	$\text{H}_2\text{O}$ (25-700) $\text{NO}_x$ (50-700) $\text{CO}_2$ (50-700)
Cu/CNT-Cit	3.3 (25-125)	6.2 (125-195)	14.6 (195-265)	23.2 (265-500)	6.4 (600-1000)	53.8	100 endo	165 endo	240 endo	285 endo		$\text{H}_2\text{O}$ (25-500) $\text{NO}_x$ (110-600) $\text{CO}_2$ (150-1000)

Table 4 summarizes the data of TA and MS analysis for all precursors and Mo/CNT samples. It is well known that in ammonium heptamolybdate solutions, molybdenum can form monomeric or polymeric forms, the ratio between which is controlled by pH and the Mo concentration in the solution [61]. So, for the synthesis of Mo/CNT-PA sample ammonium heptamolybdate was dissolved in an aqueous solution of ammonia (pH = 12) instead of water (pH = 6). In such conditions, monomeric species  $\text{MoO}_4^{2-}$  are expected in the impregnation solution. The decomposition behavior of Mo/CNT-PA is generally like the one of Mo/CNT-P (Table 4). However, in the case of Mo/CNT-PA, the total weight loss is significantly lower (14.5 vs. 33.1%), which points to higher stability of the CNT support against thermal degradation (Table 4).

Thus for Mo-containing samples, the marked effect of the support on the decomposition profile is observed in the case of using ammonium para-

molybdate tetrahydrate. For the supported sample (Fig. 6b), most of the decomposition occurred up to 400 °C while for unsupported compound the completion of the decomposition was delayed until 470 °C. In contrast to  $(\text{NH}_4)_6\text{Mo}_7\text{O}_{24}\cdot 4\text{H}_2\text{O}$ , the thermal decomposition of Mo citrate complexes practically is not affected by support.

The extent of the CNT support degradation depends on the Mo precursor type (Fig. 7). The temperature of the beginning of the CNT support decomposition decreases from 500 to 300 °C in the case of the introduction of Mo in the material (Fig. 7a). The use of ammonia solution instead of water during the impregnation can reduce the negative effect of the metal presence and increase the thermal stability of the support (Fig. 7b).

Thus features of the thermal genesis of metal-carbon materials, *ceteris paribus*, are determined by the nature of the metal precursor. The interrelated effects were observed: on the one hand, the influence of the support on the decomposition

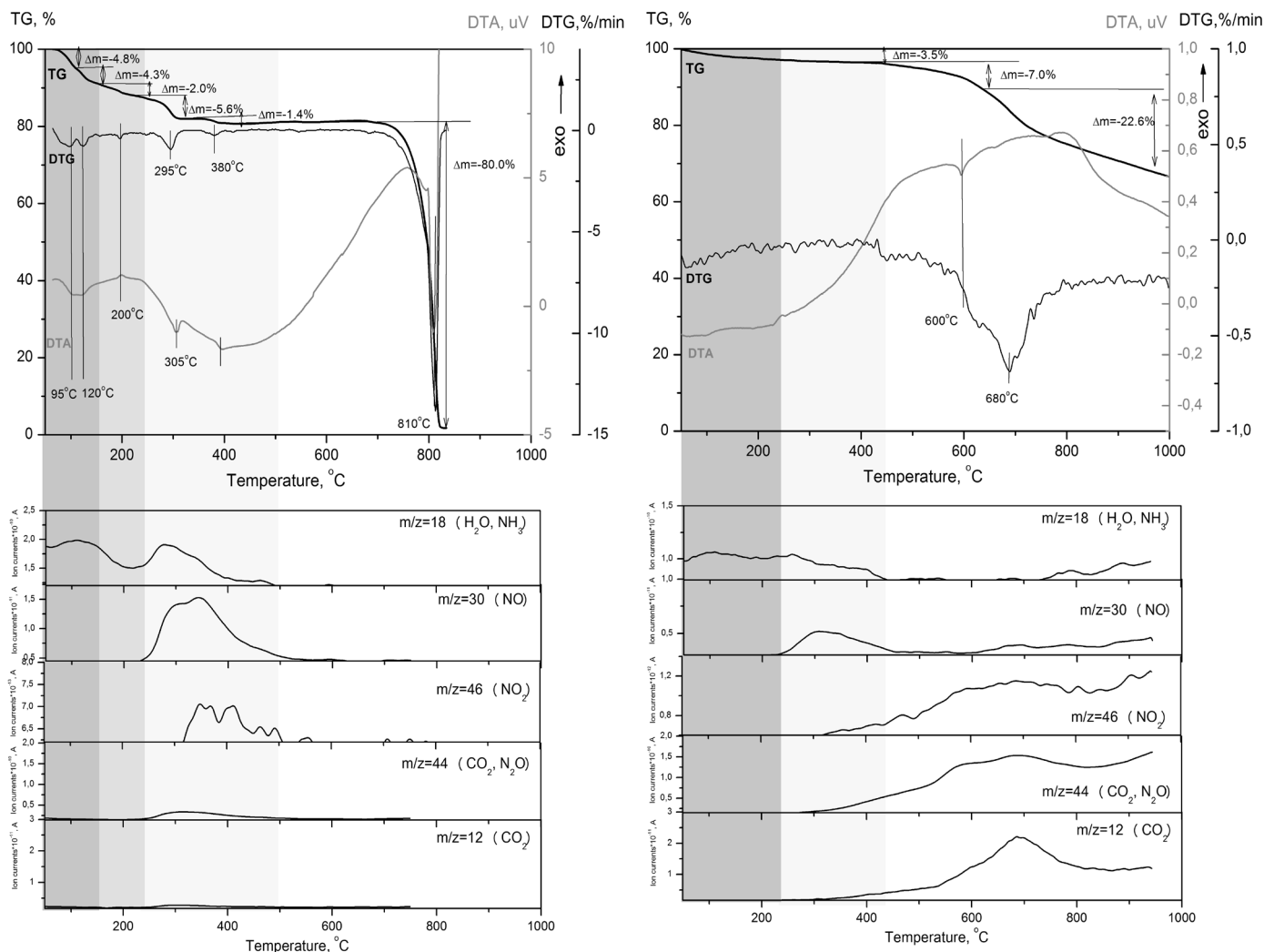


Fig. 6. TG, DTG, DSC and MS curves of bulk (a) and CNT supported (b)  $(\text{NH}_4)_6\text{Mo}_7\text{O}_{24}\cdot 4\text{H}_2\text{O}$ .

**Table 4**  
TA and MS data for the decomposition of bulk and CNT supported Mo precursor

Sample	Weight loss ( $\Delta m_i$ ), corresponding to different stages of decomposition (range of $\Delta T$ , °C), and total weight loss ( $\Delta m_{\Sigma}$ ) at 1000 °C, %					DTG peak temperature and type of thermal effect (exo/endo), °C					Evolved gas products in different temperature ranges ( $\Delta T$ , °C)	
	$\Delta m_1$	$\Delta m_2$	$\Delta m_3$	$\Delta m_4$	$\Delta m_5$	$\Delta m_{\Sigma}$	T <sub>1</sub>	T <sub>2</sub>	T <sub>3</sub>	T <sub>4</sub>		T <sub>5</sub>
(NH <sub>4</sub> ) <sub>6</sub> Mo <sub>7</sub> O <sub>24</sub> ·4H <sub>2</sub> O	4.8 (25-110)	4.3 (110-160)	2.0 (160-250)	5.6 (250-350)	1.4 (350-500)	18.1	95 endo	120 endo	200 exo	295 endo	380 endo	H <sub>2</sub> O (25-500) NH <sub>3</sub> (25-500) NO <sub>x</sub> (250-500)
Mo/CNT-P	3.5 (25-450)	7.0 (450-640)	22.6 (640-1000)			33.1	680 endo					H <sub>2</sub> O (25-450) NH <sub>3</sub> (25-450) NO (230-450) NO <sub>2</sub> (300-1000) CO <sub>2</sub> (300-1000)
Mo/CNT-PA*	1.3 (25-140)	1.4 (140-400)	11.8 (400-1000)			14.5	70 endo	200 endo	680 endo			H <sub>2</sub> O (25-500) NH <sub>3</sub> (25-500) NO (230-500) NO <sub>2</sub> (300-1000) CO <sub>2</sub> (300-1000)
Citrate complex	21.1 (25-170)	17.0 (170-215)	17.0 (215-290)	33.6 (290-1000)		88.7	145 endo	190 endo	230 endo			H <sub>2</sub> O (25-700) NO <sub>x</sub> (150-700) CO <sub>2</sub> (150-1000)
Mo/CNT-Cit	12.1 (25-165)	16.3 (165-275)	21.3 (275-540)	13.6 (540-1000)		63.2	130 exo	230 exo	350 exo			H <sub>2</sub> O (25-600) NO <sub>x</sub> (100-600) CO <sub>2</sub> (150-1000)

\* for synthesis of the Mo/CNT-PA sample, ammonium heptamolybdate was dissolved in an aqueous solution of ammonia (pH = 12) instead of water (pH = 6).

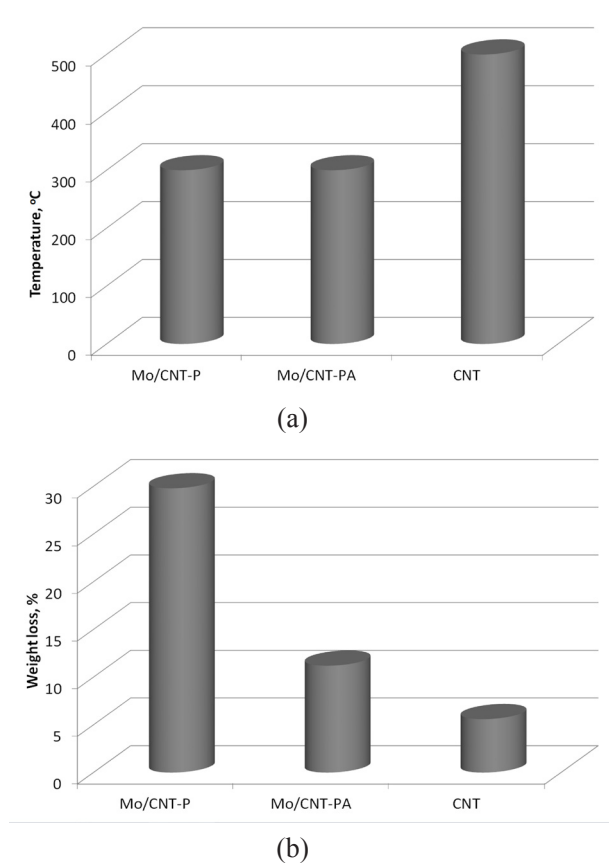


Fig. 7. The temperature of the beginning of CO<sub>2</sub> evolution (a) and weight loss (b) due to the oxidation/decomposition of CNT support during the thermal treatment of the nanocomposite: effect of Mo precursor type.

parameters of the metal salts, on the other hand, the influence of the metal salt on the behavior of the thermal degradation of the carbon support. As a rule, the deposition of the studied salts on CNTs «Taunit» led to the facilitation of their transformation manifested in a decrease in the temperature of the beginning and end of the decomposition process. The observed promoting effect may be due to the higher dispersion of salt particles on the surface of the support. A decrease in the decomposition temperature may indicate a weak metal-support interaction (MSI) in the M-CNT system as opposed to the observed strong MSI for M-Al<sub>2</sub>O<sub>3</sub> and M-CeO<sub>2</sub> samples [3, 5]. The introduction of salt reduces the resistance of the carbon system to thermal degradation, the degree of which depends on the type of a metal precursor used. In addition to different decomposition temperatures of the metal compounds, the determining factors are different catalytic activity of metals in the oxidation reactions of organic substrates, as well as the composition of gases released during the decomposition. Among the studied metals, cerium compounds have the highest reactivity. It was in their presence that the lowest temperatures of the onset of the CNT matrix

degradation were observed (Figs. 3a, 5a, 7a). The stability of the CNT support against thermal degradation enhanced in the following sequence of metal cations: Ce < Cu < Mo < pristine and metal precursor anions: nitrate < chloride < sulfate (Tables 3–5, Figs. 3a, 5a, 7a). The following active metal precursors (a water solution of Ce(NO<sub>3</sub>)<sub>3</sub>·6H<sub>2</sub>O, a water solution of Cu(NO<sub>3</sub>)<sub>2</sub>·3H<sub>2</sub>O and an ammonia solution of (NH<sub>4</sub>)<sub>6</sub>Mo<sub>7</sub>O<sub>24</sub>·4H<sub>2</sub>O)) were selected for the advanced synthesis of nanosized MO<sub>x</sub>/CNT catalysts. Based on the obtained data, a sample calcination temperature of 600 °C was chosen. At this temperature, the decomposition of the corresponding metal precursors is ensured, and the degradation of the carbon support is avoided.

#### 4. Conclusions

To develop new catalysts based on CNMs with supported metal oxide nanoparticles for oxidative transformations of sulfur compounds, a series of metal oxide nanoparticle-decorated carbon nanotubes (MO<sub>x</sub>/CNTs, M = Ce, Mo, Cu) were prepared by incipient wetness impregnation and studied by thermoanalytical techniques coupled with mass spectrometry. The effect of the CNT support on the decomposition pattern of metal precursors used in the preparation of MO<sub>x</sub>/CNTs, as well as the influence of modification on the thermal properties of CNTs was elucidated. During thermal treatment of as-prepared samples under inert atmosphere from room temperature to 1000 °C the thermal decomposition of the metal precursor supported on CNTs, as well as the degradation of the carbon matrix occur. It was established that the decomposition of metal precursors supported on CNTs mostly shifted to low temperature compared with the bulk active metal precursor. The stability of CNT support against thermal degradation enhanced in the following row of metal cations: Ce < Cu < Mo < pristine and metal anions of precursor: nitrate < chloride < sulfate. The thermal treatment at 600 °C and appropriate active metal precursors (water solution of Ce(NO<sub>3</sub>)<sub>3</sub>·6H<sub>2</sub>O, water solution of Cu(NO<sub>3</sub>)<sub>2</sub>·3H<sub>2</sub>O and ammonia solution of (NH<sub>4</sub>)<sub>6</sub>Mo<sub>7</sub>O<sub>24</sub>·4H<sub>2</sub>O)) were selected for the advanced synthesis of nanosized MO<sub>x</sub>/CNT catalyst.

#### Acknowledgments

This study was financially supported by the Russian Science Foundation (Project No. 19-13-00129). This study was accomplished using the research facilities of the Federal Research Center of Coal and Coal Chemistry of SB RAS.

## References

- [1]. F. Zaera, *Chem. Soc. Rev.* 42 (2013) 2746–2762. DOI: [10.1039/c2cs35261c](https://doi.org/10.1039/c2cs35261c)
- [2]. C.E. Figueira, P.F. Moreira, R. Giudici, R.M.B. Alves, M. Schmal, *Appl. Catal. A Gen.* 550 (2018) 297–307. DOI: [10.1016/j.apcata.2017.11.019](https://doi.org/10.1016/j.apcata.2017.11.019)
- [3]. Z.R. Ismagilov, E.V. Matus, I.Z. Ismagilov, O.B. Sukhova, S.A. Yashnik, V.A. Ushakov, M.A. Kerzhentsev, *Catal. Today* 323 (2019) 166–182. DOI: [10.1016/j.cattod.2018.06.035](https://doi.org/10.1016/j.cattod.2018.06.035)
- [4]. P. Mäki-Arvela, D.Y. Murzin, *Appl. Catal. A Gen.* 451 (2013) 251–281. DOI: [10.1016/j.apcata.2012.10.012](https://doi.org/10.1016/j.apcata.2012.10.012)
- [5]. E.V. Matus, L.B. Okhlopkova, O.B. Sukhova, I.Z. Ismagilov, M.A. Kerzhentsev, Z.R. Ismagilov, *J. Nanoparticle Res.* 21 (2019). DOI: [10.1007/s11051-018-4454-5](https://doi.org/10.1007/s11051-018-4454-5)
- [6]. I.Z. Ismagilov, E.V. Matus, D.V. Nefedova, V.V. Kuznetsov, S.A. Yashnik, M.A. Kerzhentsev, Z.R. Ismagilov, *Kinet. Catal.* 56 (2015) 394–402. DOI: [10.1134/S0023158415030064](https://doi.org/10.1134/S0023158415030064)
- [7]. E.V. Matus, D.V. Nefedova, O.B. Sukhova, I.Z. Ismagilov, V.A. Ushakov, S.A. Yashnik, A.P. Nikitin, M.A. Kerzhentsev, Z.R. Ismagilov, *Kinet. Catal.* 60 (2019) 496–507. DOI: [10.1134/s0023158419040074](https://doi.org/10.1134/s0023158419040074)
- [8]. M. Gao, N. Jiang, Y. Zhao, C. Xu, H. Su, S. Zeng, *J. Rare Earths.* 34 (2016) 55–60. DOI: [10.1016/S1002-0721\(14\)60577-9](https://doi.org/10.1016/S1002-0721(14)60577-9)
- [9]. W. Ahmed, H.S. Ahmed, H.S. El-Sheshtawy, N.A. Mohamed, A.I. Zahran, *J. Fuel Chem. Technol.* 44 (2016) 853–861. DOI: [10.1016/s1872-5813\(16\)30039-1](https://doi.org/10.1016/s1872-5813(16)30039-1)
- [10]. H. Wang, X. Wang, J. Zheng, F. Peng, H. Yu, *Chinese J. Catal.* 35 (2014) 1687–1694. DOI: [10.1016/S1872-2067\(14\)60104-2](https://doi.org/10.1016/S1872-2067(14)60104-2)
- [11]. J.P. Tessonnier, O. Ersen, G. Weinberg, C. Pham-Huu, D.S. Su, R. Schlögl, *ACS Nano* 3 (2009) 2081–2089. DOI: [10.1021/nn900647q](https://doi.org/10.1021/nn900647q)
- [12]. J. Wang, X. Quan, S. Chen, H. Yu, G. Liu, *J. Hazard. Mater.* 368 (2019) 621–629. DOI: [10.1016/j.jhazmat.2019.01.095](https://doi.org/10.1016/j.jhazmat.2019.01.095)
- [13]. Z. Zhao, H. Zou, W. Lin, *J. Rare Earths.* 31 (2013) 247–250. DOI: [10.1016/S1002-0721\(12\)60266-X](https://doi.org/10.1016/S1002-0721(12)60266-X)
- [14]. S-K. Ryu, W-K. Lee, S-J. Park, *Carbon Lett.* 5 (2004) 180–185
- [15]. Y. Lin, D.W. Baggett, J.W. Kim, E.J. Siochi, J.W. Connell, *ACS Appl. Mater. Interfaces.* 3 (2011) 1652–1664. DOI: [10.1021/am200209e](https://doi.org/10.1021/am200209e)
- [16]. A. Mahajan, A. Kingon, Á. Kukovecz, Z. Konya, P.M. Vilarinho, *Mater. Lett.* 90 (2013) 165–168. DOI: [10.1016/j.matlet.2012.08.120](https://doi.org/10.1016/j.matlet.2012.08.120)
- [17]. Z. Ismagilov, S. Yashnik, M. Kerzhentsev, V. Parmon, A. Bourane, F.M. Al-Shahrani, A.A. Hajji, O.R. Koseoglu, *Catal. Rev. Sci. Eng.* 53 (2011) 199–255. DOI: [10.1080/01614940.2011.596426](https://doi.org/10.1080/01614940.2011.596426)
- [18]. W. Jiang, D. Zheng, S. Xun, Y. Qin, Q. Lu, W. Zhu, H. Li, *Fuel* 190 (2017) 1–9. DOI: [10.1016/j.fuel.2016.11.024](https://doi.org/10.1016/j.fuel.2016.11.024)
- [19]. X. Zhang, Y. Tang, S. Qu, J. Da, Z. Hao, *ACS Catal.* 5 (2015) 1053–1067. DOI: [10.1021/cs501476p](https://doi.org/10.1021/cs501476p)
- [20]. Y. Gao, R. Gao, G. Zhang, Y. Zheng, J. Zhao, *Fuel* 224 (2018) 261–270. DOI: [10.1016/j.fuel.2018.03.034](https://doi.org/10.1016/j.fuel.2018.03.034)
- [21]. W. Zhang, H. Zhang, J. Xiao, Z. Zhao, M. Yu, Z. Li, *Green Chem.* 16 (2014) 211–220. DOI: [10.1039/c3gc41106k](https://doi.org/10.1039/c3gc41106k)
- [22]. N.M. Meman, B. Zarenezhad, A. Rashidi, Z. Hajjar, E. Esmaeili, *J. Ind. Eng. Chem.* 22 (2015) 179–184. DOI: [10.1016/j.jiec.2014.07.008](https://doi.org/10.1016/j.jiec.2014.07.008)
- [23]. N. Mohammadi Meman, M. Pourkhalil, A. Rashidi, B. ZareNezhad, *J. Ind. Eng. Chem.* 20 (2014) 4054–4058. DOI: [10.1016/j.jiec.2014.01.004](https://doi.org/10.1016/j.jiec.2014.01.004)
- [24]. Z.R. Ismagilov, M.A. Kerzhentsev, S.A. Yashnik, S.R. Khairulin, A. V. Salnikov, V.N. Parmon, A. Bourane, O.R. Koseoglu, *Eurasian Chem. Tech. J.* 17 (2015) 119–128. DOI: [10.18321/ectj202](https://doi.org/10.18321/ectj202)
- [25]. S.A. Yashnik, A.V. Salnikov, M.A. Kerzhentsev, A.A. Saraev, V.V. Kaichev, L.M. Khitsova, Z.R. Ismagilov, J. Yamin, O.R. Koseoglu, *Kinet. Catal.* 58 (2017) 58–72. DOI: [10.1134/S0023158417010128](https://doi.org/10.1134/S0023158417010128)
- [26]. S.A. Yashnik, M.A. Kerzhentsev, A. V. Salnikov, Z.R. Ismagilov, A. Bourane, O.R. Koseoglu, *Kinet. Catal.* 56 (2015) 466–475. DOI: [10.1134/S0023158415040205](https://doi.org/10.1134/S0023158415040205)
- [27]. W.A.W.A. Bakar, R. Ali, A.A.A. Kadir, W.N.A.W. Mokhtar, *Fuel Process. Technol.* 101 (2012) 78–84. DOI: [10.1016/j.fuproc.2012.04.004](https://doi.org/10.1016/j.fuproc.2012.04.004)
- [28]. S. Sahebian, S.M. Zebarjad, J. Vahdati Khaki, A. Lazzeri, *Int. Nano Lett.* 6 (2016) 183–190. DOI: [10.1007/s40089-016-0185-8](https://doi.org/10.1007/s40089-016-0185-8)
- [29]. C.T. Hsieh, J.Y. Lin, *Adv. Mater. Res.* 55–57 (2008) 545–548. DOI: [10.4028/www.scientific.net/amr.55-57.545](https://doi.org/10.4028/www.scientific.net/amr.55-57.545)
- [30]. P.M. Masipa, T. Magadzu, B. Mkhondo, *S. Afr. J. Chem.* 66 (2013) 173–178
- [31]. H.M. Elnabawy, J. Casanova-Chafer, B. Anis, M. Fedawy, M. Scardamaglia, C. Bittencourt, A.S.G. Khalil, E. Llobet, X. Vilanova, *Beilstein J. Nanotechnol.* 10 (2019) 105–118. DOI: [10.3762/bjnano.10.10](https://doi.org/10.3762/bjnano.10.10)
- [32]. R. Rajarao, R.P. Jayanna, V. Sahajwalla, B.R. Bhat, *Procedia Mater. Sci.* 5 (2014) 69–75. DOI: [10.1016/j.mspro.2014.07.243](https://doi.org/10.1016/j.mspro.2014.07.243)
- [33]. A. Corma, P. Concepción, M. Boronat, M.J. Sabater, J. Navas, M.J. Yacaman, E. Larios, A.

- Posadas, M.A. López-Quintela, D. Buceta, E. Mendoza, G. Guilera, A. Mayoral, *Nat. Chem.* 5 (2013) 775–81. DOI: [10.1038/nchem.1721](https://doi.org/10.1038/nchem.1721)
- [34]. K.S. Khashan, G.M. Sulaiman, R. Mahdi, *Artif. Cell. Nanomed. B.* 45 (2017) 1699–1709. DOI: [10.1080/21691401.2017.1282498](https://doi.org/10.1080/21691401.2017.1282498)
- [35]. K.S. Khashan, M.S. Jabir, F.A. Abdulameer, *J. Phys. Conf. Ser.* 1003 (2018). DOI: [10.1088/1742-6596/1003/1/012100](https://doi.org/10.1088/1742-6596/1003/1/012100)
- [36]. B. Małecka, A. Łącz, E. Drozd, A. Małecki, *J. Therm. Anal. Calorim.* 119 (2015) 1053–1061. DOI: [10.1007/s10973-014-4262-9](https://doi.org/10.1007/s10973-014-4262-9)
- [37]. M.J. Tiernan, E.A. Fesenko, P.A. Barnes, G.M.B. Parkes, M. Ronane, *Thermochim. Acta.* 379 (2001) 163–175. DOI: [10.1016/S0040-6031\(01\)00614-1](https://doi.org/10.1016/S0040-6031(01)00614-1)
- [38]. Z. Wu, X. Cai, Z. Yang, *J. Nanoparticle Res.* 17 (2015) 1–8. DOI: [10.1007/s11051-015-3134-y](https://doi.org/10.1007/s11051-015-3134-y)
- [39]. H. Li, H. Xu, J. Wang, *J. Nat. Gas Chem.* 20(2011) 1–8. DOI: [10.1016/S1003-9953\(10\)60156-9](https://doi.org/10.1016/S1003-9953(10)60156-9)
- [40]. Z.R. Ismagilov, S.A. Yashnik, N.V. Shikina, E.V. Matus, O.S. Efimova, A.N. Popova, A.P. Nikitin, *Eurasian Chem. Tech. J.* 21 (2019) 291–302. DOI: [10.18321/ectj886](https://doi.org/10.18321/ectj886)
- [41]. C.A. Strydom, C.P.J. van Vuuren, *J. Therm. Anal.* 32 (1987) 157–160. DOI: [10.1007/BF01914558](https://doi.org/10.1007/BF01914558)
- [42]. S. Xue, W. Wu, X. Bian, Y. Wu, *J. Rare Earths.* 35 (2017) 1156–1163. DOI: [10.1016/j.jre.2017.06.001](https://doi.org/10.1016/j.jre.2017.06.001)
- [43]. R. Farra, F. Girgsdies, W. Frandsen, M. Hashagen, R. Schlögl, D. Teschner, *Catal. Letters.* 143 (2013) 1012–1017. DOI: [10.1007/s10562-013-1085-4](https://doi.org/10.1007/s10562-013-1085-4)
- [44]. N. Audebrand, N. Guillou, J.P. Auffrédic, D. Louër, *Thermochim. Acta.* 286 (1996) 83–87. DOI: [10.1016/0040-6031\(96\)02944-9](https://doi.org/10.1016/0040-6031(96)02944-9)
- [45]. M.F.P. da Silva, J.R. Matos, P.C. Isolani, *J. Therm. Anal. Calorim.* 94 (2008) 305–311. DOI: [10.1007/s10973-007-8906-x](https://doi.org/10.1007/s10973-007-8906-x)
- [46]. L. Tai, P.A. Lessing, *J. Mater. Res.* 7 (1992) 502–510. DOI: [10.1557/JMR.1992.0502](https://doi.org/10.1557/JMR.1992.0502)
- [47]. I.A. Farbun, I. V. Romanova, T.E. Terikovskaya, D.I. Dzanashvili, S.A. Kirillov, *Russ. J. Appl. Chem.* 80 (2007) 1798–1803. DOI: [10.1134/S1070427207110031](https://doi.org/10.1134/S1070427207110031)
- [48]. P. Wicinska, *J. Therm. Anal. Calorim.* 123 (2016) 1419–1430. DOI: [10.1007/s10973-015-5075-1](https://doi.org/10.1007/s10973-015-5075-1)
- [49]. M. Getsova, D. Todorovsky, V. Enchev, I. Wawer, *Monatshefte Fur Chemie.* 138 (2007) 389–401. DOI: [10.1007/s00706-007-0624-3](https://doi.org/10.1007/s00706-007-0624-3)
- [50]. I.V. Morozov, K.O. Znamenkov, Y.M. Korenev, O.A. Shlyakhtin, *Thermochim. Acta.* 403 (2003) 173–179. DOI: [10.1016/S0040-6031\(03\)00057-1](https://doi.org/10.1016/S0040-6031(03)00057-1)
- [51]. T. Cseri, S. Békássy, G. Kenessey, G. Liptay, F. Figueras, *Thermochim. Acta.* 288 (1996) 137–154. DOI: [10.1016/s0040-6031\(96\)03037-7](https://doi.org/10.1016/s0040-6031(96)03037-7)
- [52]. J. Paulik, F. Paulik, M. Arnold, *J. Therm. Anal.* 34 (1988) 1455–1466. DOI: [10.1007/BF01914370](https://doi.org/10.1007/BF01914370)
- [53]. M. Nafees, M. Ikram, S. Ali, *Dig. J. Nanomater. Biostructures.* 10 (2015) 635–641.
- [54]. Y. Yu, *Asian J. Chem.* 19 (2007) 2023–2028.
- [55]. M. Kamruddin, P.K. Ajikumar, S. Dash, R. Krishnan, A.K. Tyagi, K. Krishan, *J. Therm. Anal.* 48 (1997) 277–286. DOI: [10.1007/BF01979271](https://doi.org/10.1007/BF01979271)
- [56]. Z. Wang, G. Marin, G.F. Naterer, K.S. Gabriel, *J. Therm. Anal. Calorim.* 119 (2015) 815–823. DOI: [10.1007/s10973-014-3929-6](https://doi.org/10.1007/s10973-014-3929-6)
- [57]. A. Biedunkiewicz, M. Krawczyk, U. Gabriel-Polrolniczak, P. Figiel, *J. Therm. Anal. Calorim.* 116 (2014) 715–726. DOI: [10.1007/s10973-013-3582-5](https://doi.org/10.1007/s10973-013-3582-5)
- [58]. G. Ciembroniewicz, R. Dziembaj, R. Kalicki, *J. Therm. Anal.* 27 (1983) 125–138. DOI: [10.1007/BF01907328](https://doi.org/10.1007/BF01907328)
- [59]. E. Filipek, I. Rychlowska-Himmel, A. Paczesna, *J. Therm. Anal. Calorim.* 109 (2012) 711–716. DOI: [10.1007/s10973-012-2224-7](https://doi.org/10.1007/s10973-012-2224-7)
- [60]. A.I. Tarasova, A.Yu. Postnikov, P.I. Gavrilova, *Combust. Explos. Shock Waves* 35 (1999) 514–517. DOI: [10.1007/bf02674495](https://doi.org/10.1007/bf02674495)
- [61]. E.V. Matus, L.T. Tsykoza, Z.R. Ismagilov, V.V. Kuznetsov, *Chemistry Sustain. Dev.* 11 (2003) 167–171.